ACS APPLIED MATERIALS & INTERFACES

Research Article

www.acsami.org

Novel Composite Material Polyoxovanadate@MIL-101(Cr): A Highly Efficient Electrocatalyst for Ascorbic Acid Oxidation

Diana M. Fernandes,[†] André D. S. Barbosa,[†] João Pires,[‡] Salete S. Balula,[†] Luís Cunha-Silva,*[,†] and Cristina Freire*[,†]

[†]REQUIMTE, Departamento de Química e Bioquímica, Faculdade de Ciências, Universidade do Porto, 4169-007 Porto, Portugal

[‡]Departamento de Química e Bioquímica, CQB, Faculdade de Ciências, Universidade de Lisboa, Campo Grande C8, 1749-016 Lisboa, Portugal

Supporting Information

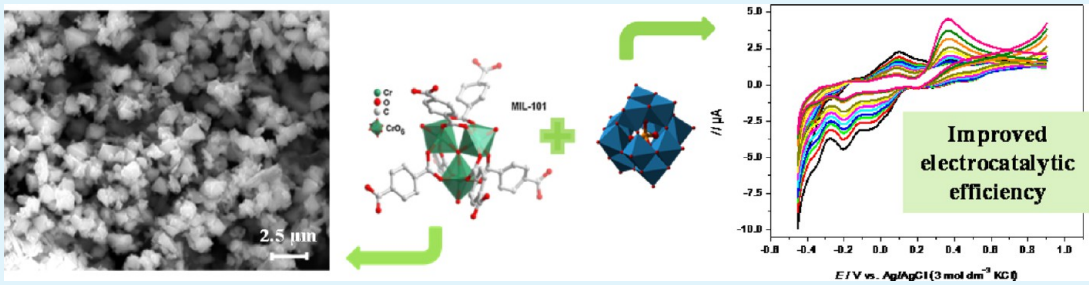

ABSTRACT: A novel hybrid composite material, $PMo_{10}V_2$@MIL-101 was prepared by the encapsulation of the tetrabutylammonium (TBA) salt of the vanadium-substituted phosphomolybdate $[PMo_{10}V_2O_{40}]^{5-}$ ($PMo_{10}V_2$) into the porous metal-organic framework (MOF) MIL-101(Cr). The materials characterization by powder X-ray diffraction, Fourier transform infrared spectra and scanning electron microscopy confirmed the preparation of the composite material without disruption of the MOF porous structure. Pyrolytic graphite electrodes modified with the original components (MIL-101(Cr), $PMo_{10}V_2$), and the composite material $PMo_{10}V_2$@MIL-101 were prepared and their electrochemical responses were studied by cyclic voltammetry. Surface confined redox processes were observed for all the immobilized materials. MIL-101(Cr) showed one-electron reduction process due to chromium centers ($Cr^{III} \rightarrow Cr^{II}$), while $PMo_{10}V_2$ presented five reduction processes: the peak at more positive potentials is attributed to two superimposed 1-electron vanadium reduction processes ($V^V \rightarrow V^{IV}$) and the other four peaks to Mo-centred two-electron reduction processes ($Mo^{VI} \rightarrow Mo^V$). The electrochemical behavior of the composite material $PMo_{10}V_2$@MIL-101 showed both MIL-101(Cr) and $PMo_{10}V_2$ redox features, although with the splitting of the two vanadium processes and the shift of the Mo- and Cr- centered processes to more negative potentials. Finally, $PMo_{10}V_2$@MIL-101 modified electrode showed outstanding enhanced vanadium-based electrocatalytic properties towards ascorbic acid oxidation, in comparison with the free $PMo_{10}V_2$, as a result of its immobilization into the porous structure of the MOF. Furthermore, $PMo_{10}V_2$@MIL-101 modified electrode showed successful simultaneous detection of ascorbic acid and dopamine.

KEYWORDS: *polyoxometalates, metal organic-framework, electrocatalysis, ascorbic acid, dopamine, electrochemistry*

INTRODUCTION

Polyoxometalates (POMs) are a type of compounds formed by bulky clusters of transition metal oxide anions and have gained increasing interest due to their application in a variety of scientific fields.[1−4] They present themselves as attractive building blocks employed in the construction of functional materials with potential electrocatalytical applications and use in molecular electronic science and in the design of electo-optical devices.[5,6] Among all their properties, the ability for reversible multi-valence reductions, leading to the formation of mixed-valence species, is extremely important as it brings about favorable electrocatalytic properties with regard to several asserted electrochemical processes.[7] Polyoxotungstates and polyoxomolybdates have been extensively used as electrocatalysts.[5] Nevertheless, the electrocatalytic performances of the parent Keggin polyanions have been considerably more studied than the polyoxovanadates. The substitution of Mo^{VI} (or W^{VI}) by V^V allows the adjustment of the electrochemical properties of the POMs[5,6] since the oxidizing ability decreases in the following order: $V^V > Mo^{IV} > W^{IV}$. Also, replacement of vanadium into POM structure give rise to species that are stable at higher pH values, which is a key factor in numerous (electro)catalytic processes.[6,8,9]

Porous tri-dimensional (3D) metal−organic frameworks (MOFs) are regarded nowadays as an auspicious type of material as their porous structures with large, regular, and

Received: October 2, 2013
Accepted: December 5, 2013
Published: December 5, 2013

accessible cages and tunnels make them prime candidates to act as support for several active chemical species. Porous MOFs can also act as nano-reactors due to their aptitude to accommodate in their pores species of catalytic interest with suitable shape and size. This type of materials can also exhibit intrinsic interesting properties; however, reports concerning their electrochemical behavior are scarce.[10,11] As far as we know, only Paes de Sousa et al.[12] studied the electrochemical behavior of MIL-101(Cr) and its respective composite materials using monovacant POMs, but no electrocatalytic applications of these composite materials were described.

Electrochemical determination of ascorbic acid (AA) has been already reported.[13,14] This compound is electroactive at different solid electrodes, however, its oxidation involves undesirable high overvoltages. Several other problems, such as poor reproducibility, sensitivity and selectivity, are also reported in the literature.[15] The known poor selectivity is due to the presence of uric acid (UA) and dopamine (DA) in real systems, which are electroactive at similar potentials as AA. With the ultimate goal of obtain efficient electrodes for AA detection, the oxidation potentials should be lowered and the respective currents increased. One effective way to accomplish this is through modification of electrode surfaces with suitable catalytic active species. Consequently, the design of new POMs with electrocatalytic activities and new strategies for their immobilization on electrode surfaces, maintaining or even enhancing their properties is a current important area of research.

This work reports the encapsulation of vanadium-substituted phosphomolybdate into the 3D porous MOF MIL-101(Cr). The composite material was characterized by several techniques and the electrochemical responses and electrocatalytic activity towards AA of both $PMo_{10}V_2$ and composite material $PMo_{10}V_2$@MIL-101 were evaluated. In addition, simultaneous detection of DA and AA was determined for $PMo_{10}V_2$@MIL-101 composite material.

EXPERIMENTAL SECTION

Materials and Instrumentation. Chromium(III) nitrate nonahydrate (Aldrich, 99%), hydrofluoric acid (Aldrich, 40−45%), terephtalic acid (Aldrich, 98%), sodium sulphate (Prolabo, 99.5%), sulphuric acid (Merck, 95-97%), acetonitrile (Panreac, 99%), dopamine (Sigma), and L-ascorbic acid (Sigma) were used as received.

Elemental analysis for P, Cr, Mo, and V were carried out by Inductively Coupled Plasma (ICP) spectrometry (Instituto Superior Técnico, Lisboa, Portugal). A Varian cary 50 Bio spectrophotometer was used to record the electronic spectra, at room temperature, in the range 190−1000 nm, using quartz cells (l = 1 cm). The Fourier transform infrared spectra (FTIR) were performed in a spectrophotometer Jasco FT/IR-460 Plus, using KBr pellets (Merck, spectroscopic grade) using a resolution of 4 cm^{-1} and 32 scans and between 400 and 4000 cm^{-1}. Scanning electron microscopy (SEM) was carried out using a high-resolution (Schottky) environmental SEM with X-ray microanalysis and backscattered electron diffraction pattern analysis (FEI Quanta 400FEG/EDAX Genesis X4M), in high-vacuum conditions, at the Centro de Materiais da Universidade do Porto (CEMUP). A thin Au layer was deposited on the top of the samples by sputtering, using the SPI Module Sputter Coater equipment.

Nitrogen (Air Liquide, 99.999%) physisorption studies were performed in a volumetric apparatus (NOVA 2200e, surface area and pore size analyzer) at −196 °C. Each experiment consisted on degassing ≈20 mg of material at 120 °C during 2.5 h at low pressure (< 0.133 Pa). The BdB-FHH method[16] was used to obtain the pore size distribution (PSD), and micropore volumes V_μ, were determined from t-plots, using an suitable nonporous reference material. The amount N_2 adsorbed at $p/p^0 \approx 0.95$[17] was used to estimate the total pore volume V_{total}. X-ray powder diffractograms were recorded with a Philips PW 1730 diffractometer with automatic data acquisition APD Phillips (v3.6B) software using a Cu anode (λ = 1.5406 Å) and 40 kV and 30 mA in the X-ray tube with a step size of 0.02° 2θ.

A suitable single-crystals of TBA salt of the vanadium-substituted phosphomolybdate was manually selected, mounted on a cryo-loop,[18] and data acquisition was carried out at 150 K on a Bruker X8 APEX II diffractometer (radiation Mo Kα graphite-monochromated with λ = 0.71073 Å) monitored by the APEX2 software package,[19] with the temperature of acquisition (150 K) set up with liquid nitrogen stream by the Oxford Cryosystems Series 700 equipment.[20] Diffraction frames were initially processed with SAINT+,[21] and the subsequent multi-scan absorption correction was performed in SADABS.[22] The crystal structure was solved with SHELXS-97[23,24] (permitting the immediate location of various heavier atoms, such as V, Mo, and P) and the successive refinements cycles have been carried out using with SHELXL-97.[23,25] Crystal data: brown prism with 0.40 × 0.29 × 0.18 mm^3, cubic, space group $I\bar{4}3m$, $a = b = c$ = 17.5885(9) Å, $\alpha = \beta = \gamma$ = 90°, V = 5441.10(5) $Å^3$.

Synthesis of Compounds. The tetra-butylammonium (TBA) salt of vanadium-substituted phosphomolybdate $[PMo_{10}V_2O_{40}]^{5-}$ (TBA-$PMo_{10}V_2$) and the porous MIL-101(Cr) were prepared using adapted procedures from literature.[26−28] The compounds were characterized by several techniques and the results obtained are in good agreement with the literature.[26,27]

The composite material was prepared through the immobilization of TBA-$PMo_{10}V_2$ into the MIL-101(Cr) structure using a modified procedure of the method reported in the literature:[29] shortly, 1.0 g of MIL-101(Cr) was added to a TBA-$PMo_{10}V_2$ solution (7.4 mM in 25 mL acetonitrile) and stirred for 4 days at room temperature. The resultant compound was filtrated, washed with acetonitrile, and left to dry under vacuum at room temperature.

Electrochemical Studies. An Autolab PGSTAT 30 potentiostat/galvanostat (EcoChimie B.V.) with a GPES software was used for cyclic voltammetry (CV) and square-wave voltammetry (SWV) studies. A three-electrode system was used where the electrodes were as follows: reference, Ag/AgCl (sat. KCl) (BAS, MF-2052); auxiliary, platinum wire (7.5 cm, BAS, MW-1032); and working, basal plane pyrolytic graphite disk (PG, ref. ACSF01315, 3.2 mm Ø, GE Quartz Europe) . The working cell was surrounded by a grounded Faraday cage and all studies were carried out at room temperature and under a argon flow. For the pH measurements was used a pH meter Basic 20^+ with a combined glass electrode (both from Crison).

Ultra-pure water (Millipore, 18.2 MΩ cm, 25°C) was used to prepare all electrolyte solutions. For electrochemical measurements was used a H_2SO_4/Na_2SO_4 buffer solution (pH = 2.5), which was prepared by mixing suitable volumes of 0.5 mol dm^{-3} Na_2SO_4 solution with a 0.2 mol dm^{-3} H_2SO_4 solution.

Prior to being used, the PG electrode was cleaned which consisted on polishing it on a microcloth polishing pad (BAS Bioanalytical Systems Inc.) with aluminium oxide (0.3 μm particle size, Buehler), Finally, the electrode was washed with ethanol and ultra-pure water and sonicated in the later in an ultrasonic bath (FUNGILAB) for 5 min. Electrode modification consisted in depositing an appropriate amount of powder of each material on the PG surface.

RESULTS AND DISCUSSION

Composite Material $PMo_{10}V_2$@MIL-101. As TBA-$PMo_{10}V_2$ was isolated in the crystalline form, it was possible to confirm its structure and molecular formula by single-crystal XRD. The cell parameters, crystalline system, and space group (see Experimental Section for more details) are identical to those reported recently and therefore confirm unequivocally the preparation of di-vanadium substituted Keggin phosphomolybdate, formulated as $(TBA)_4H[PMo_{10}V_2O_{40}]$.[30]

The preparation of the composite material $PMo_{10}V_2$@MIL-101 was performed through encapsulation of TBA-$PMo_{10}V_2$

into the pores of the MIL-101(Cr) in liquid phase (acetonitrile solution) and was monitored by UV/Vis spectroscopy. The UV/Vis spectra of the reaction solution at $t = 0$ and after 4 days of reaction are depicted in Figure S1 (see Supporting Information). After 4 days of reaction was observed a evident decrease of the absorbance of the bands at ca. 200 nm, assigned to ligand-to-metal-charge transfer transition (LMCT) from the terminal oxygen atoms to the Mo atoms ($O_t \rightarrow Mo^{VI}$) and at *ca.* 305 nm, attributed to LMCT from the bridging oxygen atoms O_b and O_c to Mo^{VI} atoms, which confirms the incorporation of $PMo_{10}V_2$ into MIL-101(Cr) framework. The POM immobilization efficiency can be calculated using the Beer–Lambert law, $A_\lambda = \varepsilon bc$ (A_λ is the absorbance at the specified wavelength, ε is the isotropic molar absorption coefficient (M^{-1} cm^{-1}), b is the path length (cm), and c is the analyte concentration (M)). To determine the isotropic molar absorption coefficient of $PMo_{10}V_2$, a set of seven solutions ($5.0 \times 10^{-7} - 1.0 \times 10^{-4}$ mol dm^{-3}) in acetonitrile was used and the value obtained was 2.09×10^4 M^{-1} cm^{-1}. This led to a $PMo_{10}V_2$ loading of 0.412 g/g of composite material and to a POM immobilization efficiency of 77%.

The integrity of the polyoxomolybdate in the MOF material framework was initially confirmed by FT-IR vibrational spectroscopy; in Figure 1, it is represented the FTIR spectrum

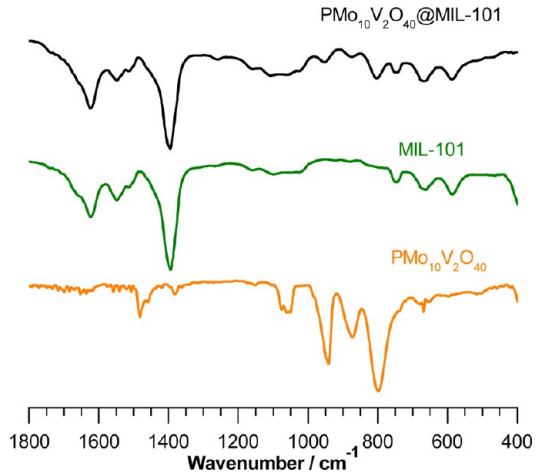

Figure 1. FT-IR spectra of $PMo_{10}V_2$, the solid support MIL-101(Cr) and the composite material ($PMo_{10}V_2$@MIL-101), shown between 1800 and 400 cm^{-1}.

of the composite material ($PMo_{10}V_2$@MIL-101) as well as those of the free components ($PMo_{10}V_2$ and MIL-101(Cr)). Spectrum of $PMo_{10}V_2$@MIL-101 shows the typical vibrational bands of the Supporting Information and various bands characteristics of the $PMo_{10}V_2$ assigned to the Mo–O_d (953 cm^{-1}), Mo–O_b–Mo (875 cm^{-1}), and Mo–O_c–Mo (803 cm^{-1}) asymmetrical stretching modes.[26]

The powder diffractograms of polyoxomolybdate ($PMo_{10}V_2O_{40}$), the MOF material MIL-101(Cr) and the $PMo_{10}V_2$@MIL-101 are depicted in Figure 2. The diffraction patterns of the isolated MIL-101(Cr) and the composite material $PMo_{10}V_2$MIL-101 are considerably identical, in both the position and in relative intensity of the main diffraction peaks, indicating that the crystalline structure of the solid support is preserved after the inclusion of the polyoxomolybdate in their pores. In fact, the main peaks are not affected and the slight alterations in intensity of few diffraction peaks

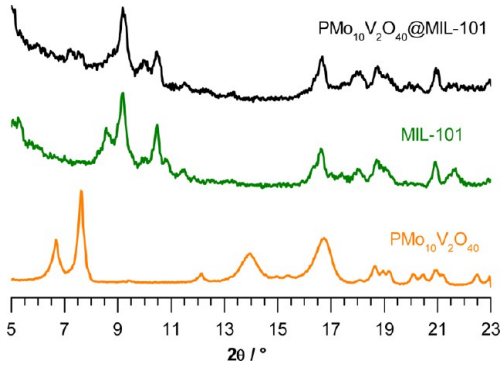

Figure 2. Powder XRD patterns of PMo10 V2, the solid support MIL-101(Cr), and the composite material (PMo10 V2@MIL-101).

(small increase in peaks at ca. 7° and the tiny decrease in the peaks around 8°, 10.5°, and 22°) in the diffractogram of $PMo_{10}V_2$@MIL-101 are a consequence of small structural and electronic rearrangements in the framework of the porous support upon the incorporation of $PMo_{10}V_2$ into the channels and cages.[28,31] Diffraction peaks due to the polyoxomolybdate $PMo_{10}V_2O_{40}$ are not observed, suggesting a homogeneous distribution of the molecular $PMo_{10}V_2$ within the MIL-101(Cr) porous structure.

The images obtained by SEM of the solid support MIL-101(Cr) and $PMo_{10}V_2$@MIL-101 (respectively, Figure S2a and S2b in Supporting Information) revealed micro-sized crystallites with similar size and shape, confirming the preservation of the MIL-101(Cr) crystalline structure upon the POM immobilization. The EDX spectrum of composite material definitely confirms the existence of Mo, V, and P from the polyoxomolybdate and Cr belonging to the MIL-101(Cr), as well as the elemental mapping analysis revealed homogeneous distribution of all these elements in the composite material confirming the uniform incorporation of the $PMo_{10}V_2$ into the porous MOF framework (Figure 3).

In Figure 4, the profile of N_2 adsorption-desorption isotherm in the initial material is mostly type I, also showing minor type IV features.[17] This result, as well as the specific surface area (Table 1) and pore size distribution (Supporting Information Figure S3) is in line with literature results.[32,33] As a consequence of the incorporation of $PMo_{10}V_2$ the specific surface area and pore volume were reduced to near 40% of the initial value and the maximum in the pore size distribution (Supporting Information Figure S3) that was verified for the lowest values is not noticed in the incorporated samples.

Electrochemical Studies. The CVs of MIL-101(Cr) immobilized at a PG electrode, in pH 2.5 H_2SO_4/Na_2SO_4 buffer solution are shown in Figure 5. Under the conditions used, a well-defined pair of peaks is observed with $E_{pc} = 0.261$ and $E_{pa} = 0.330$ V versus Ag/AgCl, attributed to the Cr^{3+}/Cr^{2+} redox process.[12] As the scan rate increases a small shoulder is also observed both in cathodic and anodic part of the cyclic voltammograms (0.436 and 0.468 V, respectively). The new process may be associated to Cr atoms with different coordination spheres due to the presence of HO^- or Cl^-.[12]

In the range of scan rates (ν) between 0.02 and 0.17 V s^{-1}, both cathodic (E_{pc}) and anodic (E_{pa}) peak potentials varied less than 0.008 V. Figure 5b depicts the plot of log i_p versus log ν for MIL-101(Cr). These results show that both cathodic (i_{pc}) and anodic (i_{pa}) peak currents were directly proportional to ν (with $r = 0.993$ and 0.991, respectively), which indicates a surface-

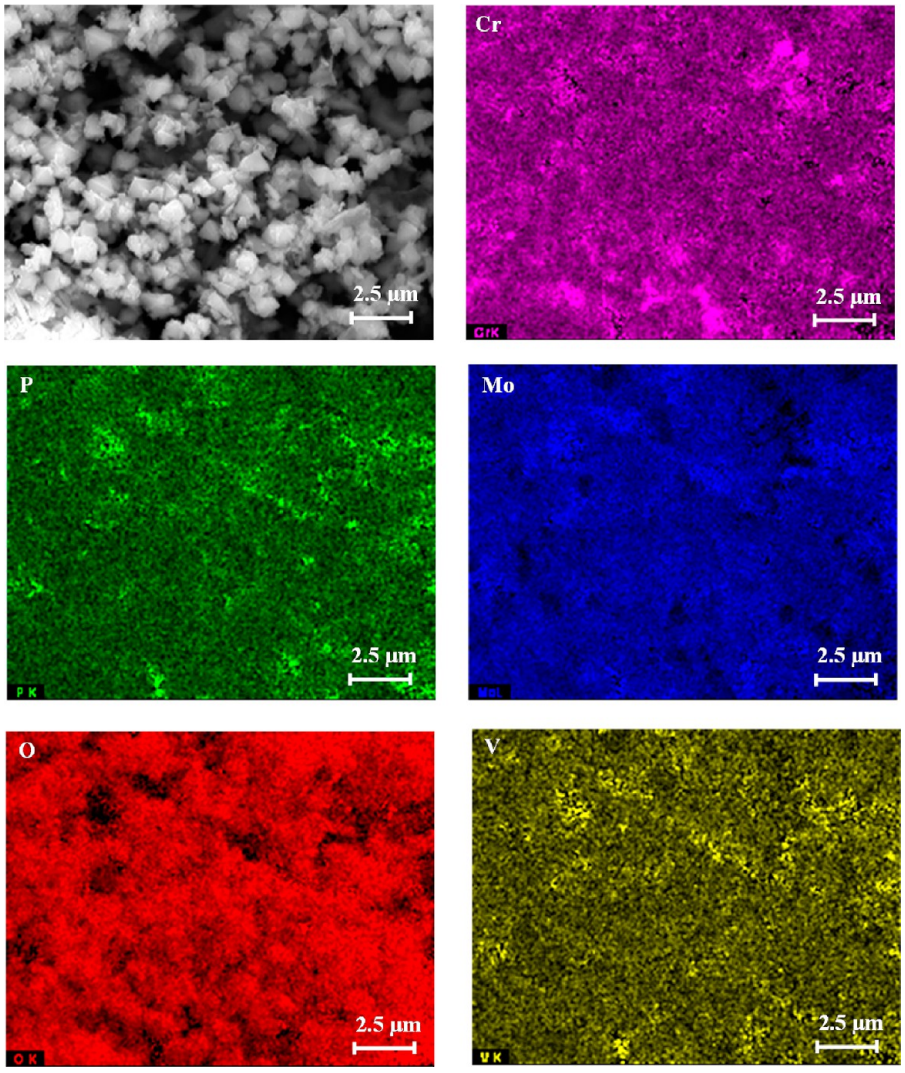

Figure 3. EDX elemental mapping images for the composite material PMo10 V2@MIL-101.

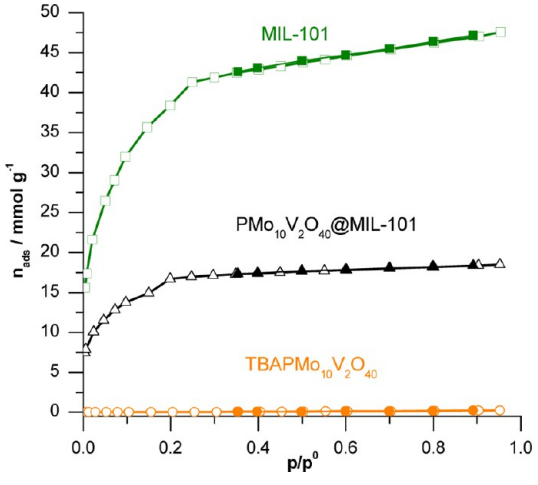

Figure 4. Nitrogen adsorption−desorption isotherms at -196° C for MIL-101(Cr) (green), $PMo_{10}V_2$, (orange), and $PMo_{10}V_2$@MIL-101 (black).

confined process.[12,34,35] Also, the peak-to-peak separations (ΔE_p) were ca. 0.069 ± 0.004 V and the ratios i_{pa}/i_{pc} were close to one (0.98 ± 0.01).

Table 1. Specific Surface Area (A_{BET}) and Total Pore Volume for the Studied Samples

compound	A_{BET} (m^2 g^{-1})	total vol. (cc g^{-1})
MIL-101	3342	1.67
TBA-$PMo_{10}V_2O_{40}$	2	0.01
$PMo_{10}V_2O_4$@MIL-101	1333	0.65

Electrochemical surface coverage (Γ) of the MIL-101(Cr) modified electrode was calculated from CV according to the equation $\Gamma = (4i_{pc}RT)/(n^2F^2\nu A)$ where i_{pc} is the cathodic peak current (amperes), R = 8.314 J K^{-1} mol^{-1}, T = 298 K, n is the number of electrons transferred (1 in this case), F is Faraday's constant, ν is the scan rate (V s^{-1}), and A is the geometric area of the electrode (0.0804 cm^2).[34] The value i_p/ν, obtained from the plot of peak currents versus scan rate (0.02 to 0.17 V s^{-1}) was used to estimate the surface coverage: Γ = 2.46 ± 0.23 × 10^{-2} nmol cm^{-2}.

The CVs of $PMo_{10}V_2$ immobilized at the PG electrode, in pH 2.5 H_2SO_4/Na_2SO_4 buffer solution are shown in Figure 6. Under the conditions used, five pairs of peaks are observed: E_{pcV} = 0.324, E_{pcMo1} = 0.093, E_{pcMo2} = −0.030, E_{pcMo3} = −0.161, and E_{pcMo4} = −0.250 V versus Ag/AgCl. Peaks Mo_1 to Mo_4 are

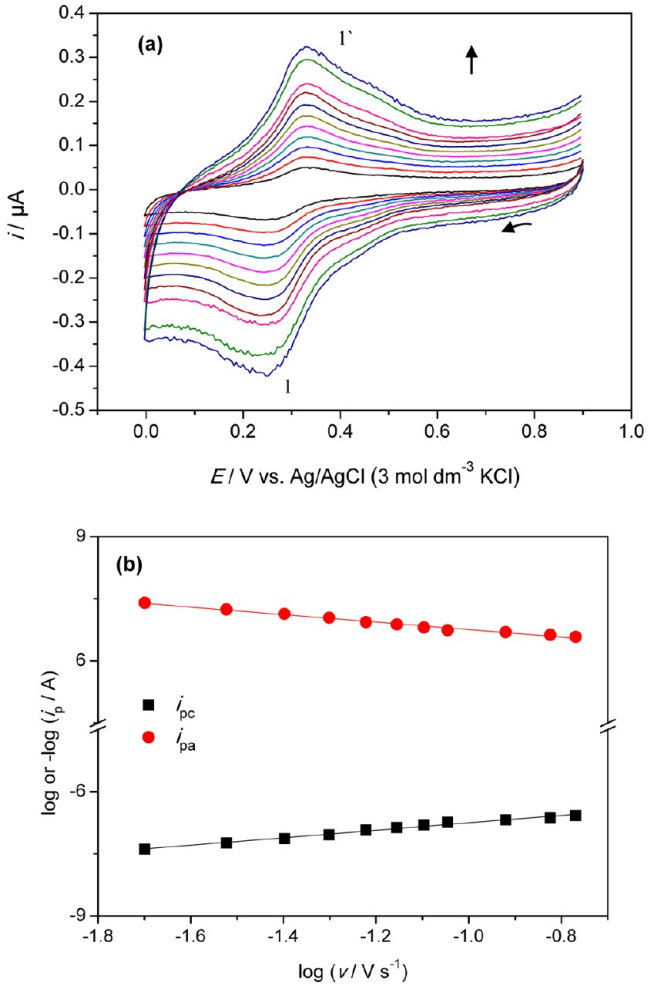

Figure 5. Cyclic voltammograms of MIL-101(Cr) immobilized at a PG electrode in pH 2.5 H_2SO_4/Na_2SO_4 buffer solution at different scan rates from 0.02 to 0.17 V s^{-1}. (a); Plots of log i_{pc} and i_{pa} vs log ν (b).

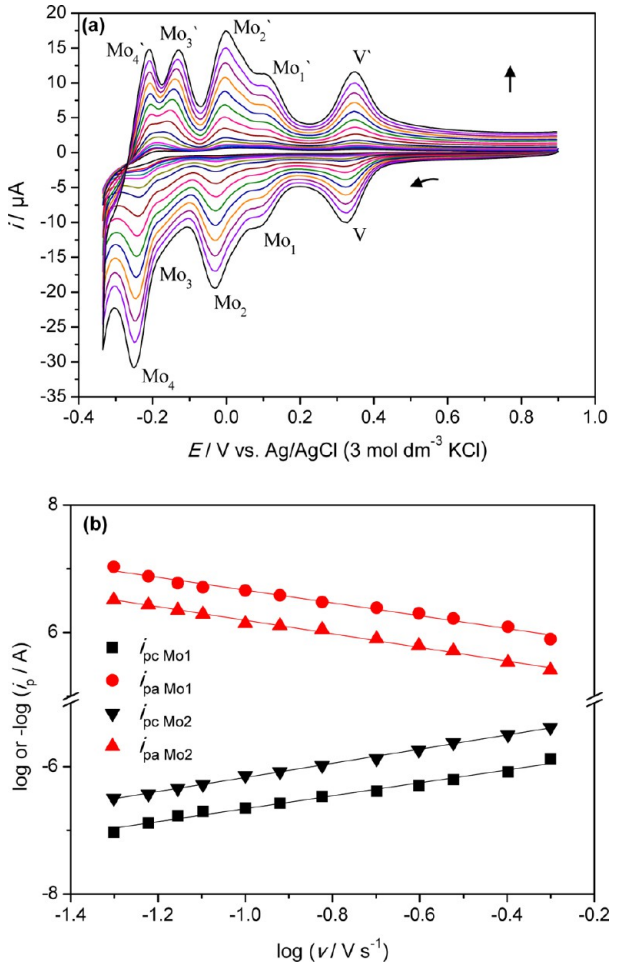

Figure 6. Cyclic voltammograms of $PMo_{10}V_2$ immobilized at a PG electrode in pH 2.5 H_2SO_4/Na_2SO_4 buffer solution at different scan rates from 0.05 to 1.0 V s^{-1} (a). Plots of log i_{pc} and i_{pa} vs log ν for Mo_1 and Mo_2 (b).

assigned to Mo-centred reduction processes ($Mo^{VI} \rightarrow Mo^{V}$) and peak V to the two vanadium reduction processes ($V^{V} \rightarrow V^{IV}$).[36]

As observed before for MIL-101(Cr), in the range of scan rates between 0.05 and 1.0 V s^{-1}, the values of peak potential did not change with ν. Figure 6b depicts the plot of log i_p versus log v for peaks Mo_1 and Mo_2, as example. Results show that i_{pc} and i_{pa} were directly proportional to scan rate (with $0.998 \geq r \geq 0.990$), which indicates a processes confined to the surface.[12,34,35] The anodic/cathodic peak-to-peak separations (ΔE_p) were ca. 0.009−0.024 V, close to the value expected for a reversible reaction in this condition (0 V). In addition, the ratios i_{pa}/i_{pc} were close to one (0.98 ± 0.02).

The widths at half height ($\Delta E_{p1/2}$) of the cathodic peaks V, Mo_1 and Mo_2 in the scan rate range used (0.048 ± 0.002, 0.038 ± 0.005, and 0.044 ± 0.004 mV, respectively) together with the expression $\Delta E_{p1/2} = 90.6/n$ mV (reversible process, n = the number of electrons) point out to three two-electron reduction processes.[36]

To calculate the electrochemical surface coverage of the $PMo_{10}V_2$ modified electrode, the cathodic peak currents of peak Mo_2 were plotted against ν (0.05 to 0.5 V s^{-1}) and the values of i_p/ν were used; for this case, the number of electrons transferred is 2 and $\Gamma = 2.34 \pm 0.22 \times 10^{-2}$ nmol cm^{-2}.

The composite $PMo_{10}V_2$@MIL-101 was immobilized on the PG electrode in the same way as for each compound individually and its electrochemical behavior in pH 2.5 H_2SO_4/Na_2SO_4 buffer solution was evaluated. The cyclic voltammograms of immobilized composite are shown in Figure 7. Under the conditions used, seven pairs of peaks are observed: $E_{pcV1} = 0.505$, $E_{pcV2} = 0.317$, $E_{pc1} = 0.195$, $E_{pcMo1} = 0.032$, $E_{pcMo2} = -0.025$, $E_{pcMo3} = -0.213$, and $E_{pcMo4} = -0.356$ V versus Ag/AgCl. From all the observed processes, it is possible to clearly identify the characteristic peaks of $PMo_{10}V_2$ and MIL-101(Cr): peaks Mo_1 to Mo_4 are assigned to the Mo-centred reduction processes ($Mo^{VI} \rightarrow Mo^{V}$) from POM, and peak 1 is attributed to the Cr centers from MIL-101(Cr). Curiously, they are shifted to less positive potentials. The other two peaks correspond to the V-based reduction processes from $PMo_{10}V_2$ that remarkably are now split into two one-electron reduction processes: one of these peaks appears at more positive potentials and the other keeps its value.

Figure 7b depicts the plot of log i_p versus log v for peaks Mo_1 and Mo_2, as example. These results also show that in the scan range 0.02 to 0.15 V s^{-1} both i_{pc} and i_{pa} were directly proportional to scan rate (with $0.998 \geq r \geq 0.991$), which indicates process confined to the surface.[34,35] Also, the values of E_p did not change with ν and the ΔE_p values vary within

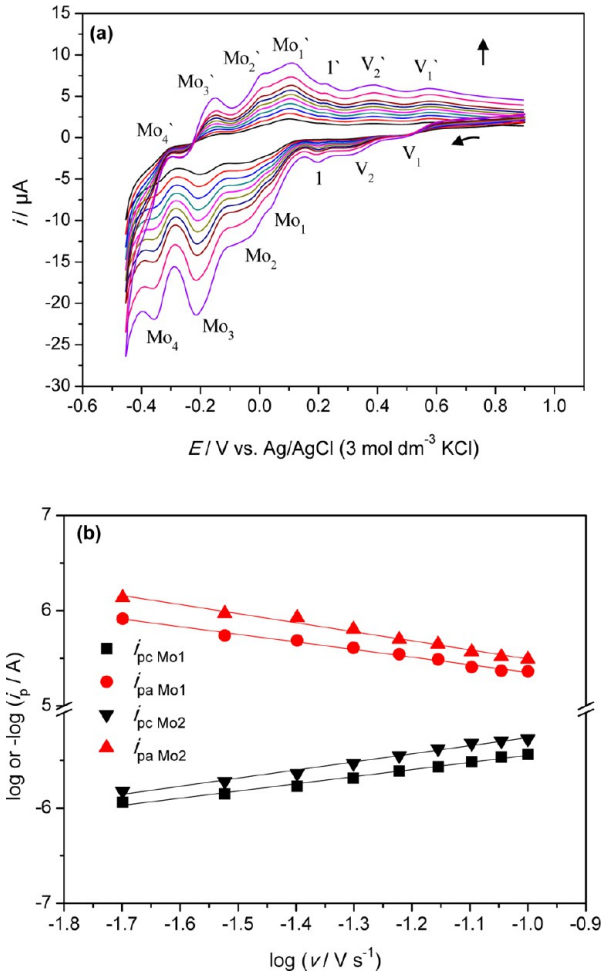

Figure 7. Cyclic voltammograms of $PMo_{10}V_2$@MIL-101 immobilized at a PG electrode in pH 2.5 H_2SO_4/Na_2SO_4 buffer solution at different scan rates from 0.02 to 0.15 V s^{-1} (a). Plots of log i_{pc} and i_{pa} vs log ν for Mo_1 and Mo_2 (b).

0.049−0.071 V. In addition, the ratios i_{pa}/i_{pc} were close to one (0.96 ± 0.05).

In order to calculate the POM electrochemical surface coverage upon immobilization into MIL-101(Cr) we used the peak Mo_2 in the CV of $PMo_{10}V_2$@MIL-10; the calculation, performed as referred before for $PMo_{10}V_2$ modified electrode, gives now $\Gamma = 2.00 \pm 0.02 \times 10^{-1}$ nmol cm^{-2}. Remarkably, this value is almost 10 times higher than the Γ value obtained for the free $PMo_{10}V_2$ modified electrode. This constitutes an outstanding advantage of the new composite relatively to the free POM: MIL-101(Cr) allowed the surface immobilization of a much larger quantity of the active species $PMo_{10}V_2$, due to its porous structure, without losing its electrochemical responses. This establishes a novel strategy to increase the quantity of electroactives species at electrode surfaces and can have very important applications in electrocatalysis and electroanalytical determinations.

Finally, the modified electrodes stability was evaluated by potential cycling of the modified electrodes for several days in pH 2.5 H_2SO_4/Na_2SO_4 buffer solution. No differences in current intensity or redox wave profiles were observed, confirming the electrochemical stability and robustness of the method used to prepare the modified electrodes.

Electrocatalytic Studies. The proof of concept for the enhanced adsorbed quantity of the active species $PMo_{10}V_2$ at the surface electrode by immobilization into the MIL-101(Cr) porous structure was done by testing the modified electrodes with $PMo_{10}V_2$ and $PMo_{10}V_2$@MIL-10 in the of ascorbic acid oxidation.

It is well-known that ascorbic acid takes part in numerous living reactions and is a vital component in the human being diet, so its detection and determination is of great importance for several industrial companies namely, those related to food, drugs, and clinical studies. POMs have been extensively exploited in electrocatalytic reactions owing to their capability to receive and give electrons to other species. The most common studied electrocatalytic reductions are the reductions of nitrite, hydrogen peroxide, chlorate, or bromate anions.[5,34,37]

Under the experimental conditions used, MIL-101(Cr) modified electrode did not show electrocatalytic properties towards ascorbic acid. Figure 8 shows the cyclic voltammograms of the $PMo_{10}V_2$ and $PMo_{10}V_2$@MIL-101 PG modified electrodes in pH 2.5 H_2SO_4/Na_2SO_4 buffer solution containing

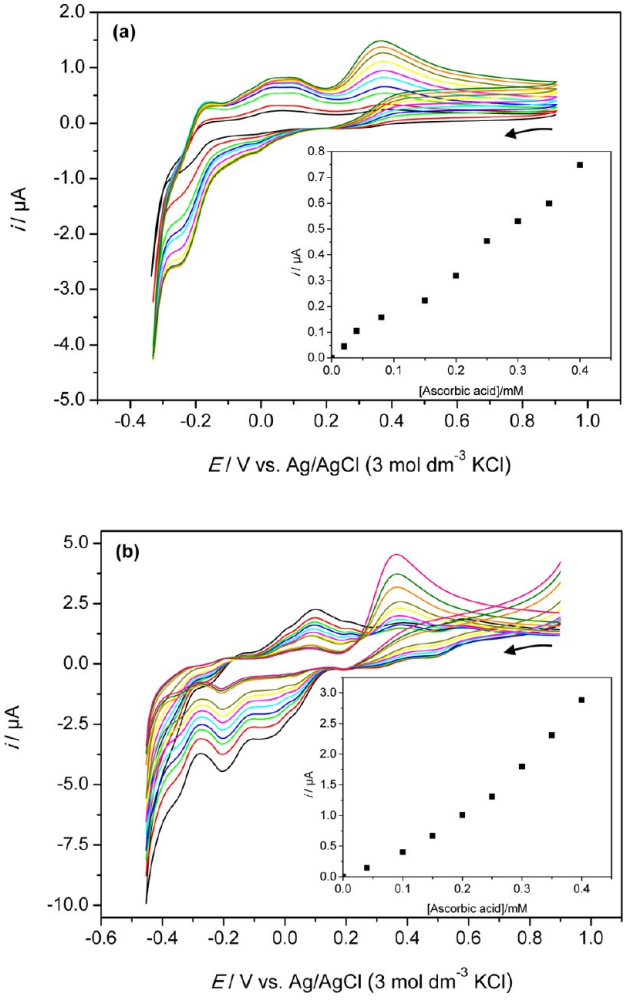

Figure 8. Cyclic voltammograms of PGE/$PMo_{10}V_2$ (a) and PGE/$PMo_{10}V_2$@MIL-101 (b) in pH 2.5 buffer solution obtained in the absence and in the presence of added concentrations of AA: (a) 0; 0.02; 0.04; 0.08; 0.15; 0.20; 0.25: 0.30; 0.35; 0.40 mM; (b) 0; 0.04; 0.10; 0.15; 0.20; 0.25: 0.30; 0.35; 0.40 mM, scan rate 0.020 Vs^{-1}. The insets show the catalytic peak current at 0.360 V vs analyte concentration.

dx.doi.org/10.1021/am4042564 | ACS Appl. Mater. Interfaces 2013, 5, 13382−13390

different AA concentrations, respectively. As can be seen, the oxidation peak currents for peak $V_1^{`}$ in $PMo_{10}V_2$ modified electrode and $V_2^{`}$ in $PMo_{10}V_2$@MIL-101 modified electrode increased with the increase of AA concentration, whereas the corresponding reduction i_p decreased, suggesting that the vanadium centers in both materials act as the active site for AA electro-oxidation.

At the bare PG electrode, ascorbic acid is oxidized at ≈0.509 V, but at these two modified electrodes, the oxidation of AA occurs at ≈0.360 V vs Ag/AgCl. The decrease in potential and increase of the AA i_{pa} shows that both $PMo_{10}V_2$ and $PMo_{10}V_2$@MIL-101 modified electrodes efficiently electrocatalyse the oxidation of AA.

The insets in Figure 8 show the plots of anodic catalytic currents versus AA concentrations at E_p = 0.360 V. As can be clearly seen, for the same amount of AA added, the peak intensity is significantly higher for $PMo_{10}V_2$@MIL-101. Quantitatively, the electrocatalytic performance of polyoxometalate can be assessed by the determination of the electrocatalytic efficiency (CAT):[37]

$$\mathrm{CAT} = 100 \times \frac{i_{p(\mathrm{POM,substrate})} - i_{p(\mathrm{POM})}}{i_{p(\mathrm{POM})}}$$

where $i_{p(POM)}$ and $i_{p(POM,\ substrate)}$ are the catalytic currents of the polyoxometalate in the absence and presence of substrate, respectively: the analysis of the corresponding current intensities lead to CAT = 734% for $PMo_{10}V_2$ and 1009% for $PMo_{10}V_2$@MIL-101. Results clearly show that the immobilization of $PMo_{10}V_2$ into the MIL-101(Cr) porous structure improved its electrocatalytic efficiency. This is a straightforward consequence of the larger amount of polyoxometalate available for the electrocatalytic reaction at the electrode surface when it is immobilized into MIL-101(Cr), compared to that of the direct immobilization of free POM at the electrode surface.

Considering the above results, selectivity tests were performed with $PMo_{10}V_2$@MIL-101 modified electrode. The major problem for AA electrochemical determination is the interference from other species such as dopamine and vice versa, because usually they coexist in real systems and their oxidation reactions, at bare electrodes, frequently occur at almost identical potentials.

In this context, and similarly to AA, the electrocatalytic oxidation of DA was performed at $PMo_{10}V_2$@MIL-101 modified electrode. Figure 9 shows the cyclic voltammograms of the $PMo_{10}V_2$@MIL-101 PG modified electrode in pH 2.5 H_2SO_4/Na_2SO_4 buffer solution containing different DA concentrations. As can be seen, the oxidation peak currents for peak $V_1^{`}$ (E_p ≈ 0.510 V vs Ag/AgCl) in $PMo_{10}V_2$@MIL-101 modified electrode increased with increasing DA concentration, suggesting that in this case the first vanadium centre acts as the active site for DA electro-oxidation (at bare PG electrode dopamine is oxidized ≈0.600 V): the electrocatalytic efficiency (CAT) towards DA oxidation is 1465%.

Square-wave voltammetry (SWV) was used to further investigate the simultaneous electrocatalytic behavior of DA and AA at $PMo_{10}V_2$@MIL-101 PG modified electrode. Figure 10a shows the SWV curves at bare and $PMo_{10}V_2$@MIL-101 PG modified electrode for DA oxidation (0.05 mM) in a solution containing 0.5 mM AA. Only one weak and broad peak was observed at the bare PGE, while at the modified electrode two oxidation peaks are observed that corresponds to AA and DA oxidation at 0.341 and 0.523 V, respectively.

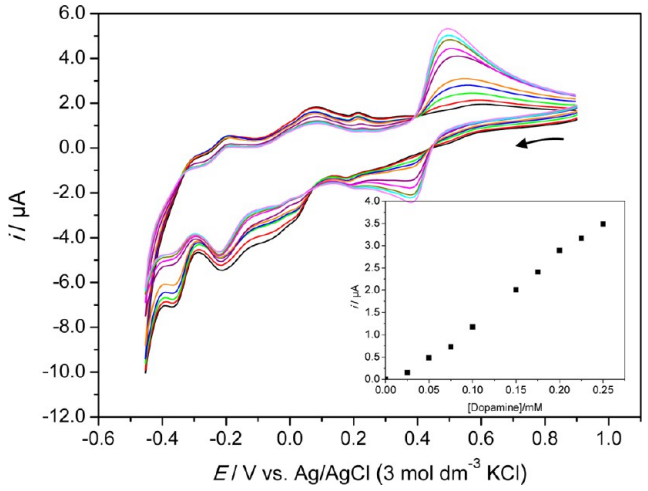

Figure 9. Cyclic voltammograms of PGE/$PMo_{10}V_2$@MIL-101 in pH 2.5 buffer solution obtained in the absence and in the presence of added concentrations of DA: 0; 0.025; 0.050; 0.075; 0.10; 0.15; 0.175: 0.20; 0.225; 0.25 mM, scan rate 0.050 Vs^{-1}.

Since the peaks of AA and DA could be resolved, SWV was also used to determine AA (or DA) while the concentration of DA (or AA) was kept constant. Figure 10b shows that the i_{pa} of AA increases linearly (i = 79.7c_{AA} + 3.87, r = 0.995) with the increasing concentration of AA in the presence of DA. Similar results were obtained for determination of DA (i = 393.9c_{DA} + 4.96, r = 0.990) in the presence of AA (Figure 10c). These results show that $PMo_{10}V_2$@MIL-101 PG modified electrode displayed good sensing performance for the detection of ascorbic acid and dopamine.

CONCLUSIONS

The vanadium-substituted phosphomolybdate anion was successfully encapsulated into MIL-101(Cr) with preservation of both MOF and POM structures, giving rise to the composite material, $PMo_{10}V_2$@MIL-101. The preparation of pyrolytic graphite electrodes modified by MIL-101(Cr), $PMo_{10}V_2$, and corresponding composite material was proved to be easy to perform and fast, leading to robust and electrochemical stable modified electrodes. All modified electrodes showed surface-confined reversible reduction processes: MIL-101(Cr) showed one redox process due to chromium metal centers; $PMo_{10}V_2$ revealed five redox processes, one assigned to vanadium centers and four to Mo centers. For the composite modified electrode, the electrochemical response comprises both MIL-101(Cr) and $PMo_{10}V_2$ redox features, but with Mo- and Cr-centered processes shifted to less positive potentials and the split of the processes due to the two vanadium atoms. The calculation of the $PMo_{10}V_2$ electrochemical surface coverage directly immobilized at the electrode surface and upon immobilization into MIL-101(Cr) porous structure showed that in the latter case it is almost 10 times higher. This constitutes an outstanding advantage of the new composite material relatively to the free $PMo_{10}V_2$ and establishes a novel strategy to increase the quantity of molecular electroactive species at electrode surfaces. This very important result was proved experimentally by the observation that $PMo_{10}V_2$@MIL-101 modified electrode acted as a much more efficient electrocatalyst toward ascorbic acid oxidation than $PMo_{10}V_2$ modified electrode. More importantly, this $PMo_{10}V_2$@MIL-101 modified electrode

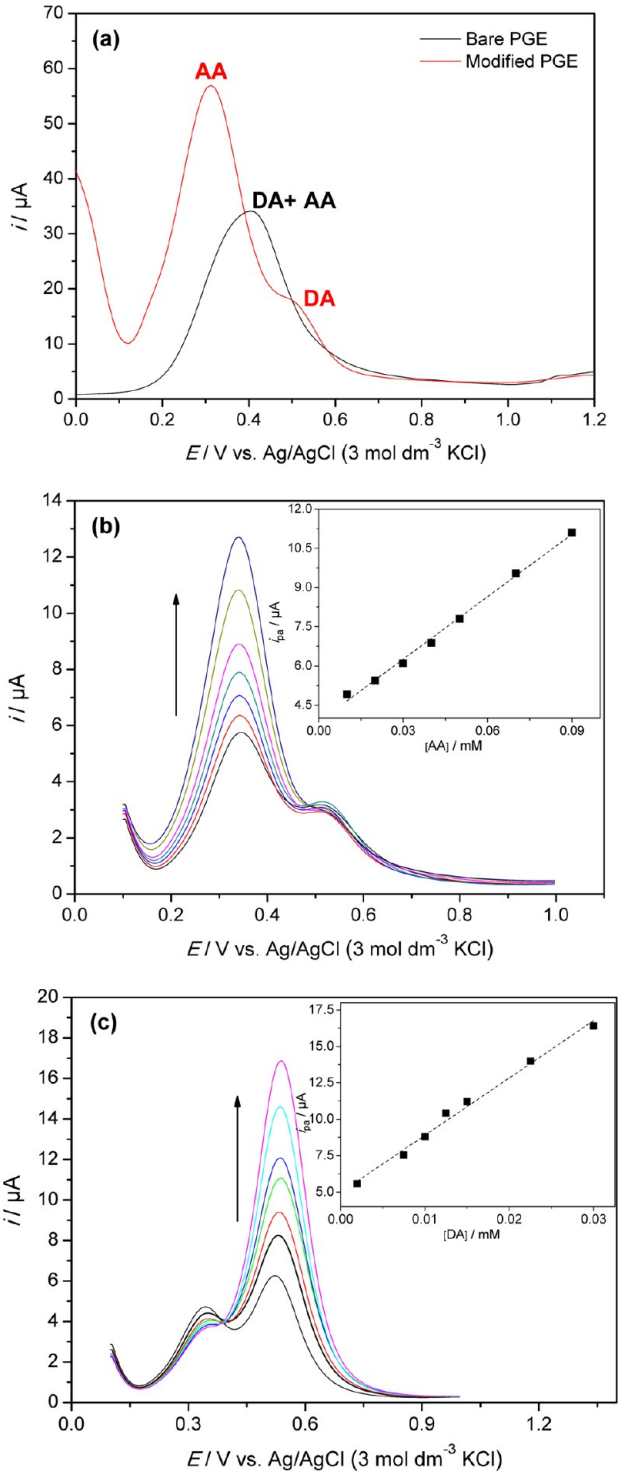

Figure 10. Square-wave voltammetric responses of 0.05 mM DA and 5 mM AA in pH 2.5 buffer solution at PGE/$PMo_{10}V_2$@MIL-101 (red) and bare PGE (black) (a). Square-wave voltammetric response in the presence of 0.001 mM of DA for different concentrations of AA: 0.01; 0.02; 0.03; 0.04; 0.05; 0.07; 0.09 mM (b). 0.01 mM of AA for different concentrations of DA: 0.002; 0.0075; 0.01; 0.0125; 0.015; 0.0225; 0.03 mM (c) in pH 2.5 buffer solution at PGE/$PMo_{10}V_2$@MIL-101.

exhibited selective determination of AA in the presence of DA and of DA in the presence of AA.

■ ASSOCIATED CONTENT

Supporting Information

(1) UV−vis spectra of the reaction solution during the preparation of the composite material $PMo_{10}V_2$@MIL-101; (2) SEM images of MIL-101 (Cr) and $PMo_{10}V_2$@MIL-101; and (3) Mesopore size distribution for MIL-101(Cr), $PMo_{10}V_2$, and $PMo_{10}V_2$@MIL-101. This material is available free of charge via the Internet at http://pubs.acs.org.

■ AUTHOR INFORMATION

Corresponding Authors

*E-mail: l.cunha.silva@fc.up.pt.
*E-mail: acfreire@fc.up.pt.

Notes

The authors declare no competing financial interest.

■ ACKNOWLEDGMENTS

The authors thank Fundação para a Ciência e a Tecnologia (FCT, Portugal) for financial support through projects PEst-C/EQB/LA0006/2011 (to REQUIMTE), PEst-OE/QUI/UI0612/2013 (to C.Q.B.), PTDC/CTM/100357/2008, Operation NORTE-07-0124-FEDER-000067−Nanochemistry and to COST Action CM-1203 PoCheMoN. D.M.F. thanks FCT for the post-doctoral fellowship SFRH/BPD/74877/2010.

■ REFERENCES

(1) Pope, M. T.; Müller, A. *Angew. Chem. Int. Ed.* **1991**, *30*, 34−48.
(2) Kholdeeva, O. A.; Maksimovskaya, R. I. *J. Mol. Catal. A* **2007**, *262*, 7−24.
(3) Misono, M. In *Studies in Surface Science and Catalysis*; Makoto, M., Ed.; Elsevier: Amsterdam, 2013; Vol. *176*, pp 97−155.
(4) Crooks, W. J.; Choppin, G. R.; Rogers, B. E.; Welch, M. J. *Nucl. Med. Biol.* **1997**, *24*, 123−125.
(5) Sadakane, M.; Steckhan, E. *Chem. Rev.* **1998**, *98*, 219−237.
(6) Lopez, X.; Bo, C.; Poblet, J. M. *J. Am. Chem. Soc.* **2002**, *124*, 12574−12582.
(7) Yang, L.-b.; Wang, X.-f.; Xie, A.-j.; Hu, G.; Shen, Y.-H. *Front. Mater. Sci. China* **2009**, *3*, 1−8.
(8) Mialane, P.; Marrot, J.; Riviere, E.; Nebout, J.; Herve, G. *Inorg. Chem.* **2001**, *40*, 44−48.
(9) Contant, R.; Abbessi, M.; Thouvenot, R.; Herve, G. *Inorg. Chem.* **2004**, *43*, 3597−3604.
(10) Babu, K. F.; Kulandainathan, M. A.; Katsounaros, I.; Rassaei, L.; Burrows, A. D.; Raithby, P. R.; Marken, F. *Electrochem. Commun.* **2010**, *12*, 632−635.
(11) Halls, J. E.; Hernan-Gomez, A.; Burrows, A. D.; Marken, F. *Dalton Trans.* **2012**, *41*, 1475−1480.
(12) de Sousa, P. M. P.; Grazina, R.; Barbosa, A. D. S.; de Castro, B.; Moura, J. J. G.; Cunha-Silva, L.; Balula, S. S. *Electrochim. Acta* **2013**, *87*, 853−859.
(13) Chethana, B. K.; Arthoba Naik, Y. *Anal. Methods* **2012**, *4*, 3754−3759.
(14) Dalmasso, P. R.; Pedano, M. L.; Rivas, G. A. *Sens. Actuators, B* **2012**, *173*, 732−736.
(15) Ammam, M.; Easton, E. B. *Electrochim. Acta* **2011**, *56*, 2847−2855.
(16) Lukens, W. W.; Schmidt-Winkel, P.; Zhao, D. Y.; Feng, J. L.; Stucky, G. D. *Langmuir* **1999**, *15*, 5403−5409.
(17) Rouquerol, J.; Rouquerol, F.; Sing, K. *Adsorption by Powders and Porous Solids, Methodology, and Applications*; Academic Press: London, 1999.
(18) Kottke, T.; Stalke, D. *J. App. Cryst.* **1993**, *26*, 615−619.
(19) Qiu, S. L.; Zhu, G. S. *Coord. Chem. Rev.* **2009**, *253*, 2891−2911.
(20) Cryopad. *Remote Monitoring and Control, Version 1.451*; Oxford Cryosystems: Oxford, U.K., 2006.

(21) SAINT+. *Data Integration Engine* v. 7.23a; Bruker AXS: Madison, WI, U.S.A., 1997−2005.
(22) Sheldrick, G. M. *SADABS* v.2.01, Bruker/Siemens Area Detector Absorption Correction Program; Bruker AXS: Madison, WI, U.S.A., 1998.
(23) Sheldrick, G. M. *Acta Cryst. A* **2008**, *64*, 112−122.
(24) Sheldrick, G. M. *SHELXS-97, Program for Crystal Structure Solution*; University of Göttingen: Göttingen, 1997.
(25) Sheldrick, G. M. *SHELXL-97, Program for Crystal Structure Refinement*; University of Göttingen: Göttingen, 1997.
(26) Himeno, S.; Ishio, N. *J. Electroanal. Chem.* **1998**, *451*, 203−209.
(27) Granadeiro, C. M.; Barbosa, A. D. S.; Silva, P.; Paz, F. A. A.; Saini, V. K.; Fires, J.; de Castro, B.; Balula, S. S.; Cunha-Silva, L. *Appl. Catal., A* **2013**, *453*, 316−326.
(28) Zhang, Y. M.; Degirmenci, V.; Li, C.; Hensen, E. J. M. *ChemSusChem* **2011**, *4*, 59−64.
(29) Maksimchuk, N. V.; Timofeeva, M. N.; Melgunov, M. S.; Shmakov, A. N.; Chesalov, Y. A.; Dybtsev, D. N.; Fedin, V. P.; Kholdeeva, O. A. *J. Catal.* **2008**, *257*, 315−323.
(30) Huang, W. L.; Todaro, L.; Yap, G. P. A.; Beer, R.; Francesconi, L. C.; Polenova, T. *J. Am. Chem. Soc.* **2004**, *126*, 11564−11573.
(31) Bromberg, L.; Diao, Y.; Wu, H. M.; Speakman, S. A.; Hatton, T. A. *Chem. Mater.* **2012**, *24*, 1664−1675.
(32) Ferey, G.; Mellot-Draznieks, C.; Serre, C.; Millange, F.; Dutour, J.; Surble, S.; Margiolaki, I. *Science* **2005**, *309*, 2040−2042.
(33) Llewellyn, P. L.; Bourrelly, S.; Serre, C.; Vimont, A.; Daturi, M.; Hamon, L.; De Weireld, G.; Chang, J. S.; Hong, D. Y.; Hwang, Y. K.; Jhung, S. H.; Ferey, G. *Langmuir* **2008**, *24*, 7245−7250.
(34) Fernandes, D. M.; Brett, C. M. A.; Cavaleiro, A. M. V. *J. Solid State Electrochem.* **2011**, *15*, 811−819.
(35) Fernandes, D. M.; Brett, C. M. A.; Cavaleiro, A. M. V. *J. Electroanal. Chem.* **2011**, *660*, 50−56.
(36) Li, C. X.; Wang, X. G.; Ma, H. Y.; Wang, F. P.; Gu, Y. *Electroanalysis* **2008**, *20*, 1110−1115.
(37) Keita, B.; Belhouari, A.; Nadjo, L.; Contant, R. *J. Electroanal. Chem.* **1995**, *381*, 243−250.